



Research Paper

“Smart” passive thermal insulation of confined natural convection heat transfer: An application to hollow construction blocks



Shahar Idan, Yuri Feldman*

Department of Mechanical Engineering, Ben-Gurion University of the Negev, P.O. Box 653, Beer-Sheva 84105, Israel

HIGHLIGHTS

- The concept of “smart” thermo-insulating materials is generalized.
- The concept is applied to thermal insulation of hollow construction blocks.
- The geometry of the optimized porous materials is determined.
- The same insulating efficiency is reported for hot and cold weather conditions.

ARTICLE INFO

Article history:

Received 21 February 2017

Revised 27 May 2017

Accepted 7 June 2017

Available online 10 June 2017

Keywords:

“smart” thermal insulation
Hollow construction blocks
Linear stability analysis
Unconnected packed beds

ABSTRACT

A method for the design of “smart” passive thermo-insulating materials based on the statistical evaluation of the confined natural convection flow in the presence of heterogeneous porous media is presented. An application of the method for the enhancement of the insulating efficiency of hollow construction blocks is discussed. Confined natural convection flow developing inside a differentially heated cavity (comprising a convenient model for the air filled cavity in the mid-core of a hollow construction block) is chosen as a computational testbed. The heterogeneous porous media in the cavity are modelled by unconnected packed beds of equi- and non-equi-sized cylinders. Each cylinder is intelligently placed in the bulk of the natural convection flow to efficiently suppress the momentum in the most energetic regions of the flow. The spatial location of each cylinder is obtained by applying linear stability analysis to the 2D natural convection flow in the presence of the modelled porous media. The flow is treated by using the mesoscale approach, implicitly resolving the flow fields in the vicinity of the immersed cylinders by the immersed boundary method. The results obtained for 2D configurations are validated for realistic 3D flows. Basic statistical evaluation of the generated porous media patterns is performed in order to generalize the developed method of design of “smart” thermo-insulating materials. It is shown that the efficiency of the thermal insulation of the porous medium is closely related to the diameter of the cylinders modelling it. This study comprises an important milestone in the design and manufacture of “smart” thermo-insulating materials from available off-the-shelf porous materials.

© 2017 Elsevier Ltd. All rights reserved.

1. Introduction

The rapid growth in energy consumption required for heating and cooling residential buildings and offices (presently accounting for more than one-third of the total energy budget in the European Community [1]) stimulates the promotion of energy saving technologies when building and maintaining premises [2]. Efficient optimization of the thermal insulation properties of hollow blocks, widely used as building elements of ventilated facades [3] and masonry structures [4], is an important step in this direction,

making it possible to enhance indoor climate control. The high popularity of hollow blocks is due to their light weight and high thermal and acoustic resistances, all achieved thanks to a large air filled cavity in the mid-core of the block. While partition of the air filled cavity can vary significantly without compromising the strength of the block (typically between 2 and 8 equal parts and up to 100 parts for the coarse and dense partitioned configurations, respectively [5]), it has a substantial effect on the convective component of heat flux passing through the hollow construction block. This is because the internal walls of a partitioned cavity suppress the intensity of convective air circulation by two physical mechanisms: first, they enforce the non-slip (zero) velocities on the internal surfaces and second, they split the flow up and, as a

* Corresponding author.

E-mail address: yurifeld@bgu.ac.il (Y. Feldman).

result, decrease the geometrical dimensions of the largest flow scales. Unfortunately, simply partitioning the air filled cavity by introducing a large number of internal walls is far from an optimal solution to improving the insulation of hollow blocks. In fact, reducing the convective heat flux in such a way is not only counterbalanced (at least partially) by the accompanying conductive and radiative heat fluxes, but also incurs the disadvantages of significant increases in weight and construction costs.

While there exists a consensus about minimizing the conductive and radiative heat fluxes by increasing the porosity of the block material [6,7] and by decreasing the radiation emissivity of recesses and the external surfaces of hollow blocks [8,9], an efficient means of minimizing convective heat flux is still sought. Therefore, in the framework of the present study the focus is only on natural convection flow and does not take into account the conduction and radiation heat transfer. The basic idea of breaking down the large scale convection cells was first established in the numerical studies of Tong and Gerner [10] and Kangni et al. [11]. Since then, the above concept has been extensively elaborated upon in a large number of studies which discussed various configurations and orientations of voids [5,12–19], investigated the effect of the thermal insulation of the boundaries of the voids [20,21] and also studied the impact of embedding obstacles into the flow bulk [22–29], to name a few.

Despite significant progress in increasing the insulating properties of hollow blocks achieved over the recent decade, the state of the art research in this area relies mostly on heuristic rather than on systematic methodology. The first attempt to reformulate the problem in terms of “smart” passive thermal insulation behavior is due to Costa [5]. It was demonstrated that protuberances inserted into the bulk of convective flow exhibit increasing self-adjusting inhibition of convection and radiation heat fluxes in the case of higher temperature differences between the hottest and the coldest walls of the hollow block. The next step towards deriving a formal methodology for the intelligent control of the confined natural convection flow by suppression of the fluctuations of the flow oscillations in the most energetic regions (as determined by linear stability analysis [30]) was recently published in the work of Gulbeg and Feldman [31]. The key idea of the study was to link the flow in the presence of patterns formed by unconnected packed beds to flow in porous media. In their analysis the authors employed the immersed boundary method to simulate the natural convection flow inside square and cubic differentially heated cavities in the presence of unconnected packed beds of equi-sized perfectly conducting circular cylinders. A collection of such unconnected cylinders embedded into the bulk of natural convection flow forms a pattern of thermo-insulating material. The pattern is not just a group of randomly embedded unconnected packed beds, rather, it is built by an iterative process to consistently suppress the flow oscillations in the most energetic flow regions as rigorously revealed by the mesoscale linear stability analysis of slightly supercritical flows and therefore forms a basis for design of “smart” thermal insulators. The thermo-insulating materials designed by the developed concept intelligently adjust to the specific flow configuration. In fact, a twofold decrease in the overall convective heat flux through the square and cubic differentially heated cavities was achieved for optimized implants of the modelled porous thermal insulator occupying only 5% of the total volume of the cavity [31].

The promising results of study [31] were obtained for only a single configuration of a porous medium and therefore require further generalization and validation. In real systems, the transport properties of a heterogeneous porous medium can be dominated by different flow scales, which requires statistical evaluation of a whole set of similar systems. The present work reports on our continuing effort aimed at further generalization of the concept of

“smart” thermal insulators in the context of decreasing convective heat flux through air filled cavities of hollow construction blocks. To generalize the concept of “smart” thermal insulators we produced a number of sets of unconnected packed cylinders of non-uniform and uniform diameters. Each set consists of 10 patterns in which each pattern comprises a model of heterogeneous porous medium. The shapes, spatial locations and porosity values of the modelled porous medium implants that provide a twofold decrease in convective heat flux are statistically evaluated based on the results obtained for natural convection flow through each pattern.

The concept of utilizing a pore level (mesoscale) approach in modelling porous media is not new and has been extensively discussed in the past few decades. Worth mentioning are the work of Martin et al. [32], who studied laminar steady 2D flow through square and triangular periodic arrays in an attempt to develop a universal model for accurately predicting the pressure drop for a wide range of Reynolds numbers; the study of Keyser et al. [33], who simulated flow through a number of beds packed with randomly shaped particles, keeping the same average particle size; the work of Sangani and Yao [34] and of Narvaez et al. [35], who focused on fluid flow through randomly packed beds of monomodal cylinders with a wide range of Reynolds numbers; and the study of Rochette and Claim [36], who simulated flow through a porous bed with abruptly varying porosity. The principal novelty of the present work is that it analyzes a number of sets of similar systems by basing on a formal linear stability analysis performed on the mesoscale level. The study aims at developing methodology that will potentially lead to the design of realistic “smart” thermo-insulators built from off-the-shelf porous materials. The objectives are: first, to perform an extensive validation and a grid independence proof of the established 2D methodology by performing direct numerical simulations (DNS) for realistic 3D configurations obtained by extrusion in the spanwise direction of the corresponding 2D patterns; and second, to address the impact of the porosity, the heterogeneity, the shape and the orientation of the modelled porous media implants on enhancement of the thermal insulation of the hollow construction blocks. It is also shown that the optimized hollow blocks operate with approximately the same insulation performance in the presence of both positive and negative temperature gradients across the block and can, therefore, be beneficial for both cooled and heated indoor environments.

2. Theoretical background and basic assumptions

We start with a general description of the concept of the design of a smart thermo-insulating material in the context of thermal insulation of hollow construction blocks. Fig. 1a shows a schematic of a typical hollow construction block which can contain two (or more) air cavities. As a result of temperature differences between the indoor and the outdoor walls of the block, natural convection flow develops in each cavity, similar to the flow observed inside differentially heated cavities (i.e. a configuration in which two opposite vertical walls are held at constant high and low temperatures, while all other walls are either perfectly conducting or insulating). To suppress the convective heat transfer, implants of porous material are installed in each cavity, as shown in Fig. 1a. An example of the shape and spatial location of an embedded implant can be seen in Fig. 1b, showing a cross section of the construction block at the middle of the cavity. It should be stressed here that unconnected packed beds of cylinders embedded into the cavities of a construction block as shown in Fig. 1a and b are only used for demonstration purposes and comprise a mesoscale model of realistic porous media, such as are further characterized in this study.

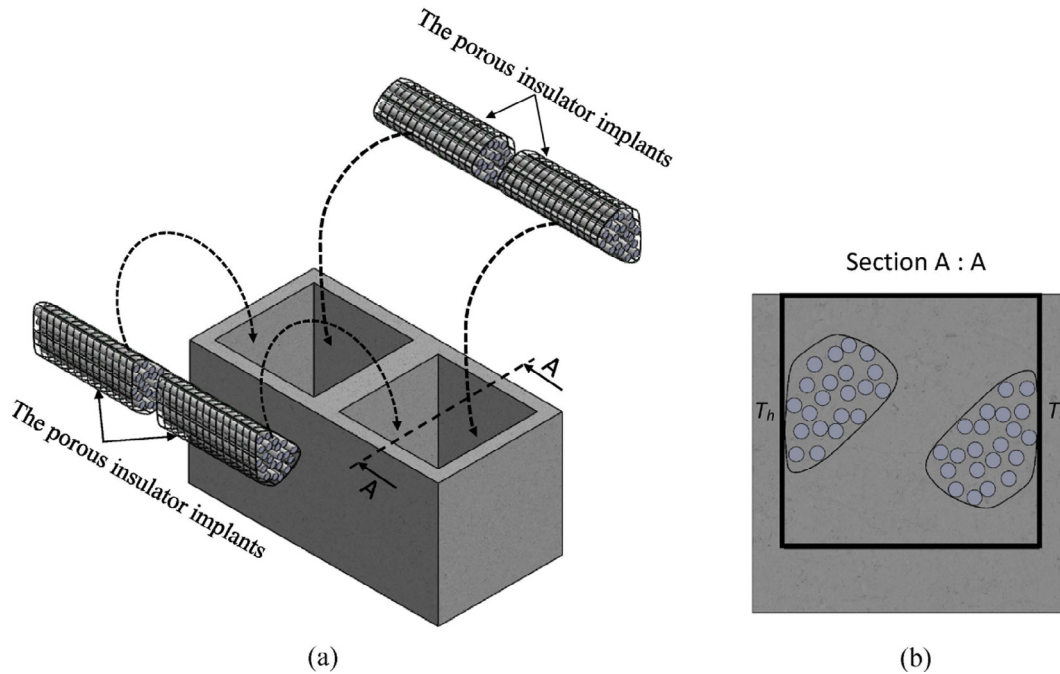


Fig. 1. A schematic of a hollow block with insulator implants of “smart” porous media: (a) general exploded view; (b) cross section view defining 2D model of differentially heated cavity.

2.1. Governing equations

The study adopts a mesoscale approach for the analysis of natural convection flow in the presence of porous media modelled by unconnected packed beds of cylindrical shape. The no-slip boundary conditions at the surfaces of the unconnected packed beds placed in the bulk of the convective flow are enforced by applying the immersed boundary (IB) method [37]. In addition, the no-slip boundary conditions are applied at all boundaries confining the differentially heated cavity. The hot and cold walls are held at constant temperatures, T_h and T_c , respectively; all other boundaries are assumed to be thermally perfectly conducting. We note that the walls of realistic construction blocks do not have precisely constant temperature and are not perfectly conducting, but, nevertheless, these assumptions are reasonable for the purpose of an optimization. Since we focus on the investigation of convective heat transfer, radiation effects are not considered. Buoyancy effects are introduced by applying the Boussinesq approximation. As a result, the unsteady natural convection flow is governed by the following system of continuity, Navier-Stokes (NS), and energy equations (Eqs. (1)–(3)), along with additional kinematic constraints that are summarized by Eqs. (4) and (5); these equations are introduced to enforce the no-slip and the determined temperature (or heat flux) boundary conditions on the surfaces of the modelled porous media.

$$\nabla \cdot \mathbf{u} = 0 \quad (1)$$

$$\frac{\partial \mathbf{u}}{\partial t} + (\mathbf{u} \cdot \nabla) \mathbf{u} = -\nabla p + \sqrt{\frac{Pr}{Ra}} \nabla^2 \mathbf{u} + \theta \vec{e}_y + \mathbf{f} \quad (2)$$

$$\frac{\partial \theta}{\partial t} + (\mathbf{u} \cdot \nabla) \theta = \frac{1}{\sqrt{PrRa}} \nabla^2 \theta + q \quad (3)$$

$$\mathbf{U}_b(\mathbf{X}_k) = \mathbf{I}(\mathbf{u}(\mathbf{x})) \quad (4)$$

$$\Theta_b(\mathbf{X}_k) = \mathbf{I}(\theta(\mathbf{x})), \quad (5)$$

where $\mathbf{u} = (u, v, w)$, p , t , and θ are the non-dimensional velocity, pressure, time and temperature variables, respectively, and \vec{e}_y is a unit vector in the vertical (y) direction. Following the works of Christon et al. [38] and Xin and Le Quere [39], the problem is scaled by L , $U = \sqrt{g\beta L \Delta T}$, $t = L/U$, and $P = \rho U^2$ for length, velocity, time, and pressure, respectively. Here, L is the length of the square differentially heated cavity, ρ is the mass density of the working fluid, g is the gravitational acceleration, β is the isobaric coefficient of thermal expansion, and $\Delta T = T_h - T_c$ is the temperature difference between the hottest and coldest boundaries. The non-dimensional temperature θ is defined as $\theta = (T - T_c)/\Delta T$. The Rayleigh, Ra , and Prandtl, Pr , numbers are $Ra = \frac{g\beta}{\nu\alpha} \Delta T L^3$ and $Pr = \nu/\alpha$, respectively, where ν is the kinematic viscosity and α is the thermal diffusivity. All the spatial derivatives in Eqs. (1)–(3) are discretized by a standard second order finite volume method; the second order backward finite difference scheme is utilized for the temporal discretization. All the linear terms are treated implicitly while all the non-linear terms are taken from the previous time step and moved to the right hand side (RHS) of Eqs. (2) and (3). The volumetric force \mathbf{f} and the heat source q , appearing as sources in Eqs. (2) and (3), reflect the impact of the immersed surfaces of the porous media on the surrounding flow. These sources are additional unknowns of the overall system of Eqs. (1)–(3), a closure of which is achieved by introducing additional kinematic constraints determined by Eqs. (4) and (5). To convey information between Lagrangian points of immersed surfaces and an Eulerian staggered grid, on which Eqs. (1)–(5) are discretized and solved, we define two adjoint operators, namely, regularization operator \mathbf{R} and interpolation operator \mathbf{I} as:

$$\mathbf{R}(\mathbf{F}^k(\mathbf{X}^k), Q^k(\mathbf{X}^k)) = \int_S (\mathbf{F}^k(\mathbf{X}^k), Q^k(\mathbf{X}^k)) \cdot \delta(\mathbf{x}_i - \mathbf{X}^k) dV_S^k, \quad (6a)$$

$$\mathbf{I}(\mathbf{u}(\mathbf{x}_i), \theta(\mathbf{x}_i)) = \int_\Omega (\mathbf{u}(\mathbf{x}_i), \theta(\mathbf{x}_i)) \cdot \delta(\mathbf{X}^k - \mathbf{x}_i) dV_{\Omega_i}. \quad (6b)$$

Here S corresponds to all the cells belonging to the immersed body surface, Ω corresponds to a group of flow domain cells located in the close vicinity of the immersed body surface, dV_S^k corresponds to

the virtual volume surrounding each Lagrangian point k , and dV_{oi} is the volume of the corresponding cell of the Eulerian flow domain, whose velocity and temperature values are explicitly involved in enforcing the boundary conditions at point k of the immersed body. Both operators use convolutions with the Dirac delta function δ to facilitate an exchange of information between the Lagrangian points of the body surface and the Eulerian grid. The discrete delta function introduced by Roma et al. [40] was used in the present study.

$$d(r) = \begin{cases} \frac{1}{6\Delta r} \left[5 - 3\frac{|r|}{\Delta r} - \sqrt{-3\left(1 - \frac{|r|}{\Delta r}\right)^2 + 1} \right] & \text{for } 0.5\Delta r \leq |r| \leq 1.5\Delta r, \\ \frac{1}{3\Delta r} \left[1 + \sqrt{-3\left(\frac{|r|}{\Delta r}\right)^2 + 1} \right] & \text{for } |r| \leq 0.5\Delta r, \\ 0 & \text{otherwise,} \end{cases} \quad (7)$$

where Δr is the cell width in the r direction.

The linear stability eigenproblem is formulated by assuming infinitesimally small perturbations of the form $\{\tilde{\mathbf{u}}(x, y), \tilde{\theta}(x, y), \tilde{p}(x, y), \tilde{\mathbf{F}}(x, y), \tilde{Q}(x, y)\}e^{\lambda t}$ around the steady state flow $\mathbf{U}, \theta, P, \mathbf{F}, Q$, as follows:

$$\lambda \tilde{\mathbf{u}} = -(\mathbf{U} \cdot \nabla) \tilde{\mathbf{u}} - (\tilde{\mathbf{u}} \cdot \nabla) \mathbf{U} - \nabla \tilde{p} + \sqrt{\frac{Pr}{Ra}} \nabla^2 \tilde{\mathbf{u}} - \tilde{\theta} \tilde{\mathbf{e}}_y + \mathbf{R}_{\tilde{\mathbf{F}}}, \quad (8a)$$

$$\lambda \tilde{\theta} = -(\mathbf{U} \cdot \nabla) \tilde{\theta} - (\tilde{\mathbf{u}} \cdot \nabla) \theta + \frac{1}{\sqrt{PrRa}} \nabla^2 \tilde{\theta} + R_{\tilde{Q}}, \quad (8b)$$

$$0 = \nabla \cdot \tilde{\mathbf{u}}, \quad (8c)$$

$$0 = \mathbf{I}(\tilde{\mathbf{u}}), \quad (8d)$$

$$0 = \mathbf{I}(\tilde{\theta}). \quad (8e)$$

The generalized eigenproblem in Eqs. (8a–e) with all homogeneous boundary conditions is then solved by applying the shift-and-invert Arnoldi iteration along with the secant method for the calculation of the critical values:

$$(\mathbf{J} - \sigma \mathbf{B})^{-1} \mathbf{B} \begin{bmatrix} \tilde{\mathbf{u}} \\ \tilde{\theta} \\ \tilde{p} \\ \tilde{\mathbf{F}} \\ \tilde{Q} \end{bmatrix} = \mu \begin{bmatrix} \tilde{\mathbf{u}} \\ \tilde{\theta} \\ \tilde{p} \\ \tilde{\mathbf{F}} \\ \tilde{Q} \end{bmatrix}, \quad \mu = \frac{1}{\lambda - \sigma}, \quad (9)$$

where \mathbf{J} is the Jacobian matrix calculated from the RHS of Eqs. (8a–e), and \mathbf{B} is the diagonal matrix whose diagonal elements corresponding to the values of $\tilde{\mathbf{u}}, \tilde{\theta}$ are equal to unity, and whose diagonal elements corresponding to $\tilde{p}, \tilde{\mathbf{F}}, \tilde{Q}$ are equal to zero (see Refs. [41,30] for more details).

2.2. Implementation details

The proposed method for the design of “smart” thermal insulators employs a linear stability analysis of natural convection flows in the presence of heterogeneous porous media, as detailed in a recent study by Gulberg and Feldman [31]. Following this work, the currently employed optimization procedure is based on minimizing the value of parameter \mathbf{A} , defined as $\mathbf{A} = |\tilde{u}_x|^2 + |\tilde{u}_y|^2$, where $|\tilde{u}_x|$ and $|\tilde{u}_y|$ are the absolute values of the perturbations¹ of the corresponding velocity components. The optimization procedure is an

iterative process, which will be briefly described here for the sake of completeness. The iterations start with the linear stability analysis based on the solution of Eqs. (8), performed for the flow within the cavity with no obstacles. As a result, the value of the critical Rayleigh number, Ra_{cr} , for the first Hopf bifurcation is obtained and two cylindrical obstacles are placed at the locations where the criterion \mathbf{A} attains its maximal value.² In the next step, the linear stability analysis is repeated for the modified flow, which is characterized by a new value of Ra_{cr} , at which a transition to unsteadiness takes place. The next pair of obstacles can again be positioned at places where the new values of \mathbf{A} reach their absolute maximum. In the present study, the above procedure is repeated until a twofold decrease in the average Nu number is achieved.³ Note that the boundary of each cylindrical obstacle is assumed to be of zero thickness; hence there is no need neither to employ any specific heat fluxes in Eqs. (3) and (8b) nor boundary conditions for the temperature determined by Eqs. (5) and (8e). As a result, the boundaries of the cylinders have no thermal resistance in the direction normal to the body surface.

The basic assumption of the optimization methodology implemented in the present study stems from the fact that the most energetic regions of the 2D convective flows predicted by the linear stability analysis coincide, with an acceptable degree of accuracy, with the corresponding regions observed in the 3D configuration built by extrusion of the corresponding 2D confinement along its normal direction. This idea is supported by the striking similarity between the spatial and temporal characteristics observed for 2D and 3D steady and bifurcated flows in differentially heated square and cubic cavities, respectively, with perfectly thermally conducting horizontal boundaries (see e.g. Ref. [42]). The above assumption was validated by the recent study of Gulberg and Feldman [31], who demonstrated about the same enhancement of the insulating efficiency of a 2D differentially heated cavity and its 3D counterpart, both optimized by embedded implants of porous media. Following the same principle, the efficiency of all the porous media patterns obtained by the 2D linear stability analysis was validated by the corresponding 3D simulations. The numerical solution of the full 3D NS equations (Eqs. (1)–(5)) was conducted by the recently developed IB solver [43]. Extensive discussion on the implementation and verification of the developed solver for thermal flows in the presence of thermally active and passive immersed bodies can be found in [43], and is omitted here for the sake of conciseness.

3. Results and discussion

Motivated by the recent work of Gulberg and Feldman [31], in which the concept of “smart” thermal insulation occupying only 5% of the overall volume of the differentially heated cavity was established, we present a further generalization of the concept by focussing on the following open questions:

- Is material porosity the dominant macro-optimization parameter of the heterogeneous porous medium distributed over the flow areas, as predicted by the linear stability analysis?
- For a given amount of porous material, what is the preferable way of suppressing the most unstable flow modes in accordance with the prescribed optimization criteria: is it by precise positioning of the finite size obstacles in the places determined in accordance with the given optimization criterion or by covering the vicinity of the determined locations with clusters of porous material modelled by evenly distributed unconnected obstacles?

¹ The intention is to the absolute values of the most critical eigenvectors as determined by the linear stability analysis.

² The obstacles always come in pairs due to the skew-symmetry of the flow.

³ The procedure can also be applied with another termination criterion.

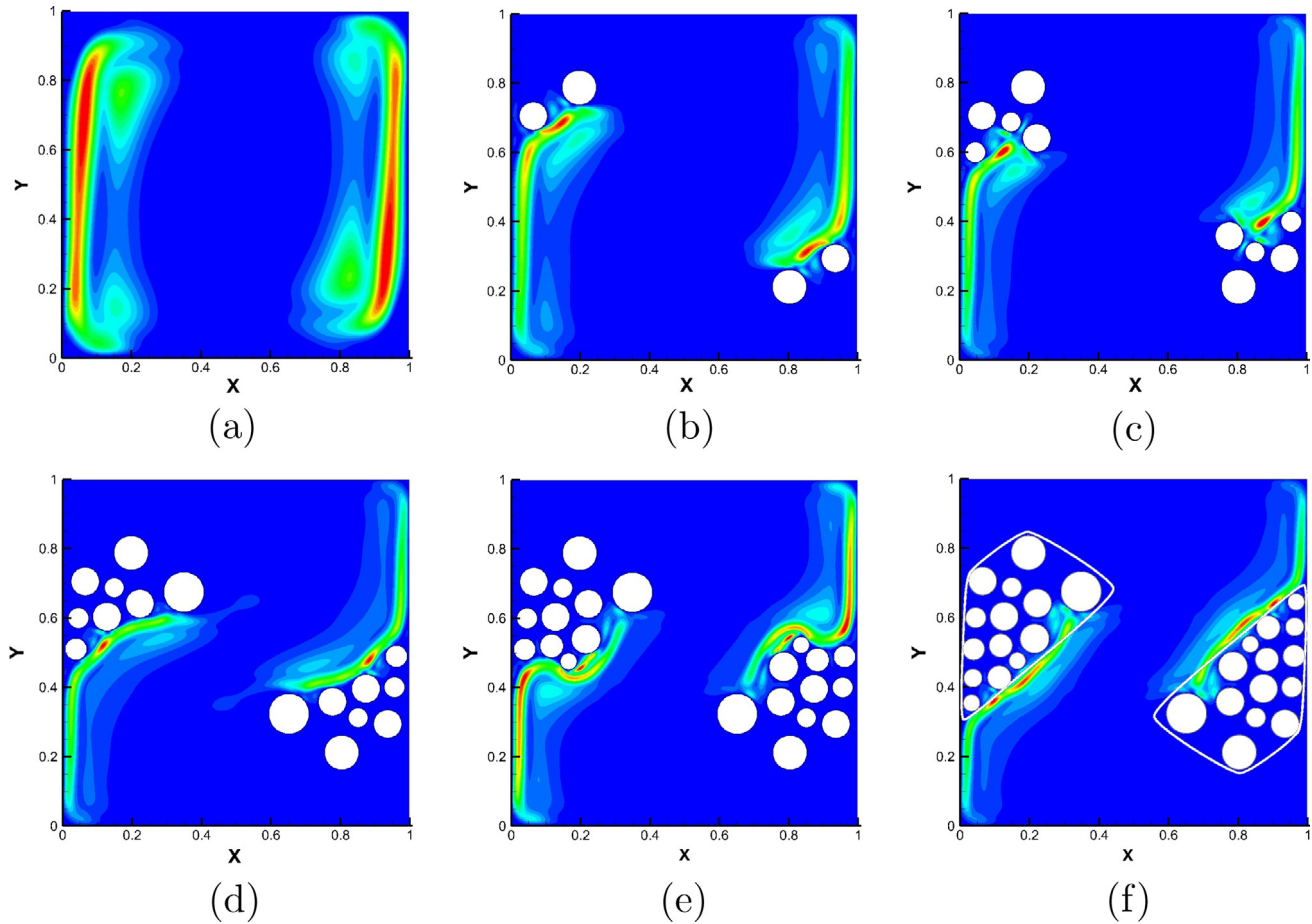


Fig. 2. Successive stages of building the pattern of a “smart” insulator characterized by the minimal porosity value, $\phi = 0.51$. The final pattern of the porous material is confined by the white solid line. The colors correspond to the distribution of the control parameter **A**. Figure (f) was obtained at $Ra = 4.39 \times 10^7$. (For interpretation of the references to color in this figure legend, the reader is referred to the web version of this article.)

- How important is the impact of the heterogeneity of the porous material?

To address the above questions we discuss the confined natural convection flow in the presence of heterogeneous porous media, modelled by clusters built of both equi- and non-equi-sized cylinders. Each pattern obtained in the present study was built based on a minimizing parameter **A** and provided a twofold decrease in the Nusselt number, \overline{Nu} , averaged over the vertical (hot and cold) boundaries of the differentially heated cavity. The patterns were grouped in sets, with 10 patterns in each set. The process of building the patterns and the analysis of the insulating properties of each set of patterns are discussed in the next two sections. Following the recent work of Gulberg and Feldman [31], all the 2D calculations that included calculation of the steady state flow and its subsequent linear stability analysis were performed on a 500×500 uniform grid, thus providing grid independence of the obtained results. All the non-dimensional results were obtained for the natural convection flow in square and cubic cavities with non-dimensional side length $L = 1$, the value of Prandtl number, $Pr = 0.71$ (corresponding to air), and the varying values of Rayleigh number, Ra . The physical values corresponding to the dimensions and temperature differences typical of realistic construction blocks are given in Appendix B.

3.1. Patterns built of non-equi-sized cylinders

To check the impact of porosity as a macro-optimization parameter determining the insulating properties of the modelled heterogeneous porous media, we start with the most general configuration and build a set of 10 different patterns, each consisting of non-equi-sized cylinders. The diameters of the cylinders in each pattern were drawn in accordance with a Gaussian distribution characterized by an average value of $D_{av} = 0.1$ and a standard deviation of $\sigma = \pm 0.02$. The patterns were built by an iterative process: first, the cylinder center was placed at the point with the maximal value of criterion **A**; second, the minimal distance between the cylinder’s boundary and the boundaries of the previously placed cylinders (for the second and subsequent placements) or the cavity walls was fixed to be at least the size of a single grid step. The second step is an intrinsic requirement of the discrete Delta functions [40] utilized in the present study for the implementation of interpolation **I** and regularization **R** operators. If the second condition could not be met, a new diameter of the subsequent cylinder was drawn. An additional limitation to be considered is related to the scenario where the distance between the point characterized by the maximal value of criterion **A** and the closest boundary is smaller than the minimal allowed value of the cylinder radius $(D_{av} - 3\sigma)/2$. In this case the location of the

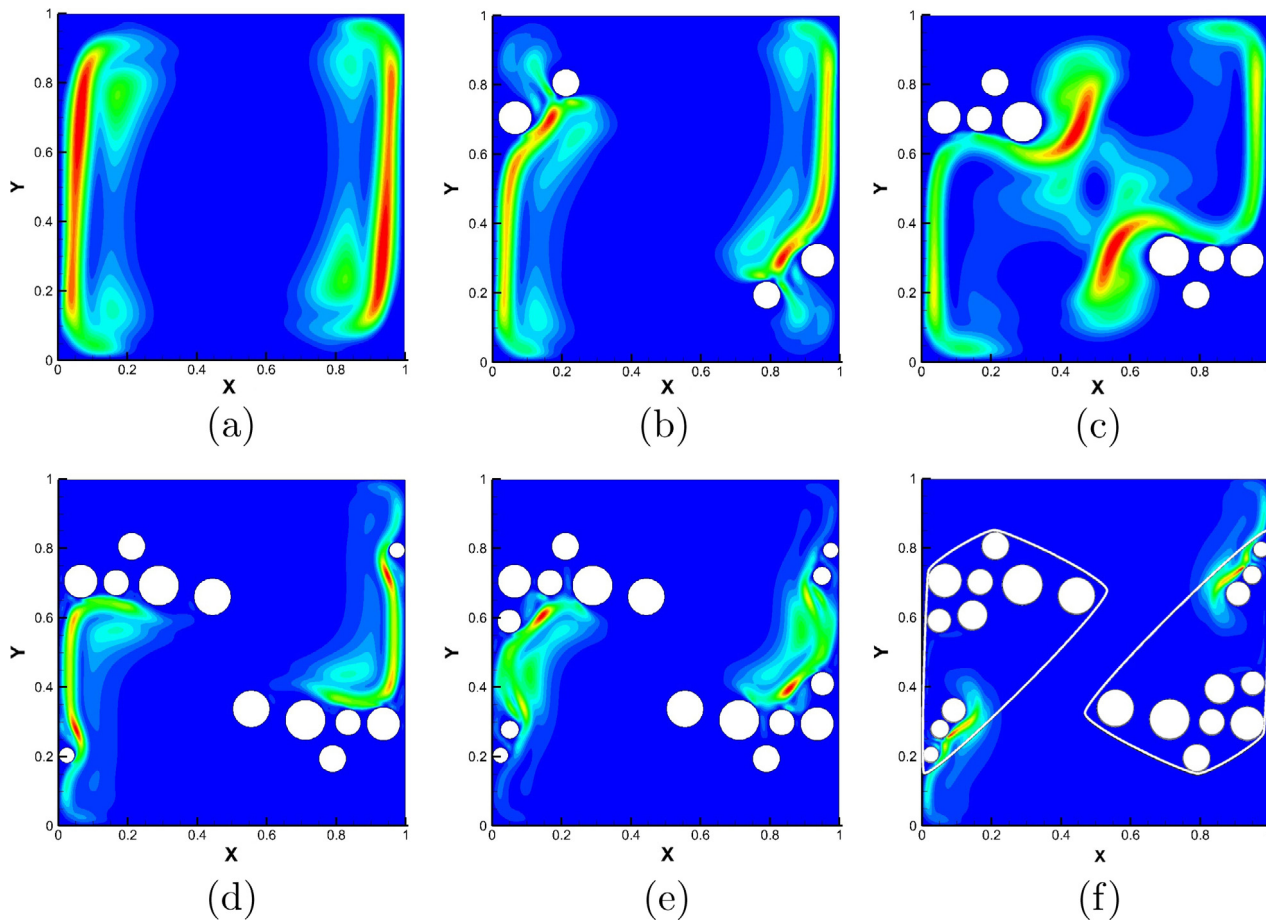


Fig. 3. Successive stages of building the pattern of a “smart” insulator characterized by the maximal porosity value, $\phi = 0.64$. The final pattern of the porous material is confined by the white solid line. The colors correspond to the distribution of the control parameter **A**. Figure (f) was obtained at $Ra = 5.13 \times 10^7$. (For interpretation of the references to color in this figure legend, the reader is referred to the web version of this article.)

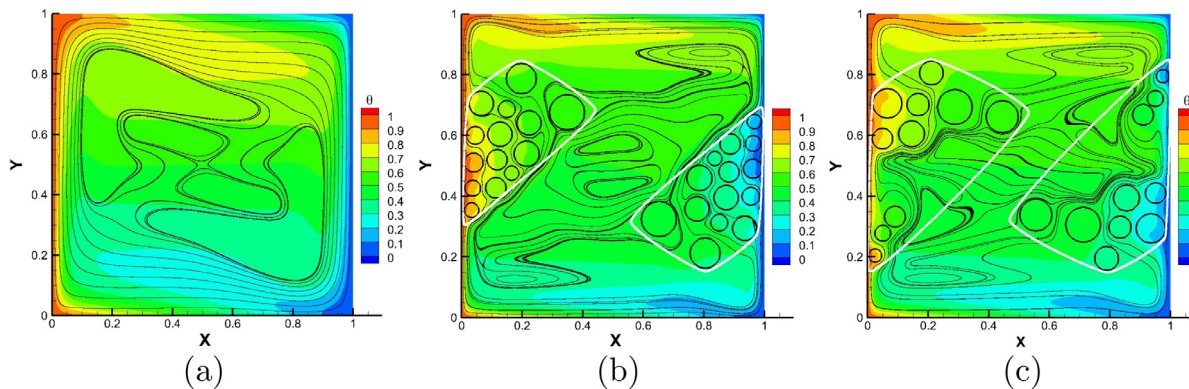


Fig. 4. Temperature distribution with superimposed streamlines for: (a) configuration without porous implants obtained for $Ra = 2.15 \times 10^6$; (b) configuration with porous implants characterized by $\phi = 0.51$ obtained for $Ra = 4.39 \times 10^7$; (c) configuration with porous implants characterized by $\phi = 0.64$ obtained for $Ra = 5.13 \times 10^7$. The transparency of the cylinders stresses the fact that their boundaries have zero thermal resistance.

next largest value of **A** is sought and the morphological structure of the new “candidate” of the porous medium implant is tested to verify that it complies with all the conditions.

In Figs. 2 and 3, two typical sequences of the construction of different porous media patterns are shown, corresponding to the porous media materials characterized by the minimal ($\phi = 0.51$) and the maximal ($\phi = 0.64$) values of porosity (from the set of 10 different patterns), respectively. Colors represent the corresponding distributions of the control parameter **A**. Note that only a single

pair of cylinders was added at each iteration (due to the skew-symmetry of the flow) and, therefore, Figs. 2 and 3 show only a number of representative configurations. The final geometry of both implants,⁴ yielding a twofold decrease in the Nusselt number, \overline{Nu} , averaged over the cavity vertical boundaries, is confined by the

⁴ The contours comprise closed cubic Bezier curves (see Appendix A for more details).

Table 1
Results obtained for the set of 10 different patterns in order of decreasing porosity, ϕ . The patterns are modelled by unconnected packed beds of cylinders of varying diameters, drawn in accordance with a Gaussian distribution characterized by an average value of $D_{av} = 0.1$ and standard deviation of $\sigma = \pm 0.02$.

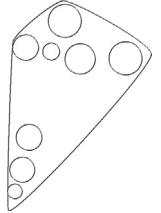
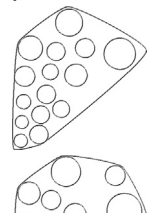
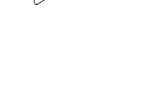
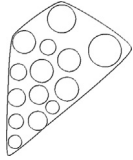
\overline{Nu} (final) @ $Ra = 2.15 \times 10^6$	Average diameter, \overline{D}	\overline{X}_c		\overline{Y}_c		Porosity, ϕ	Confinement of the porous implant
		Left	Right	Left	Right		
3.6968	0.0786	0.2028	0.7972	0.6271	0.3729	0.6388	
3.8155	0.0898	0.1962	0.8038	0.6033	0.3967	0.6358	
4.0110	0.0766	0.1891	0.8109	0.6289	0.3711	0.6322	
4.0694	0.0684	0.1732	0.8268	0.6212	0.3788	0.6265	
3.9990	0.0770	0.2127	0.7873	0.6202	0.3798	0.6250	
3.8609	0.0716	0.2075	0.7925	0.6219	0.3781	0.6222	
3.8819	0.0726	0.1744	0.8256	0.6448	0.3552	0.5981	
4.0799	0.0714	0.1796	0.8204	0.5992	0.4008	0.5239	
3.9842	0.0702	0.1413	0.8587	0.5830	0.4170	0.5148	

Table 1 (continued)

\bar{Nu} (final) @ $Ra = 2.15 \times 10^6$	Average diameter, \bar{D}	\bar{X}_c		\bar{Y}_c		Porosity, ϕ	Confinement of the porous implant
		Left	Right	Left	Right		
3.9102	0.0715	0.1718	0.8282	0.6116	0.3884	0.5078	

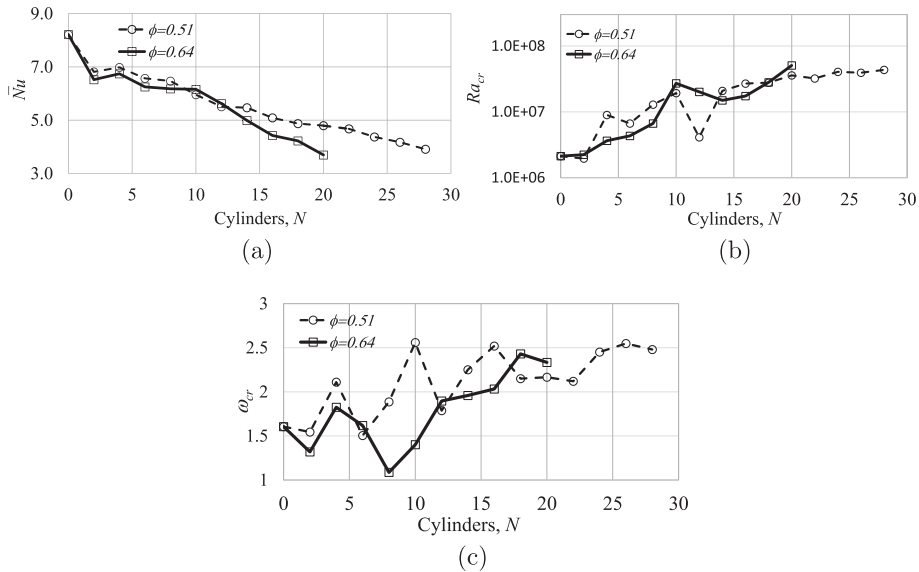


Fig. 5. Efficiency characteristics of the porous medium implants characterized by the minimal ($\phi = 0.51$) and the maximal ($\phi = 0.64$) values of porosity, ϕ , in terms of: (a) \bar{Nu} number, averaged over vertical (hot or cold) boundaries obtained for $Ra_{cr} = 2.15 \times 10^6$; (b) critical Ra_{cr} number at which the transition from steady to unsteady flow takes place via Hopf bifurcation; (c) critical angular frequency, ω_{cr} at which the transition from steady to unsteady flow takes place via Hopf bifurcation.

white curve (see Figs. 2f and 3f). Note that in the present study the porosity of the porous medium implant is defined as:

$$\phi = \left(V_p - \sum_{N_{cyl}} V_N \right) / V_p, \tag{10}$$

where V_p is the volume of the final configuration of the porous media implant.

Despite the evident differences between the structures of both patterns, a number of trends, which will be exploited for further generalization of the strategies for the design of “smart” thermally insulating materials, can be clearly recognized. First, both patterns have the shape of a bunch of grapes close to the hot vertical boundary (or the shape of an inverted bunch of grapes close to the cold vertical boundary), and are flattened in the vicinity of the vertical walls. Second, the geometric center of both configurations is much closer to the vertical compared to the horizontal walls of the cavity. Third, the convective flows that initially rise or descend along the vertical hot or cold walls, respectively, are further redirected to the cavity center. As a result, the close vicinity of the vertical walls of the cavities with embedded implants of porous medium is characterized by a more uniform distribution of the temperature (see Fig. 4). This, in turn, results in lower temperature gradients and, as a consequence, in lower values of the local Nu number. It is remarkable that the same trends were also observed for all other

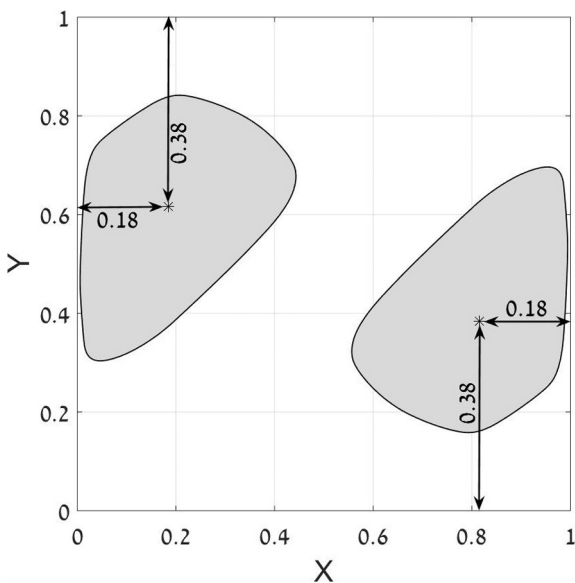


Fig. 6. Averaged confinement and spatial location of the optimized implant of porous medium inside differentially heated square cavity.

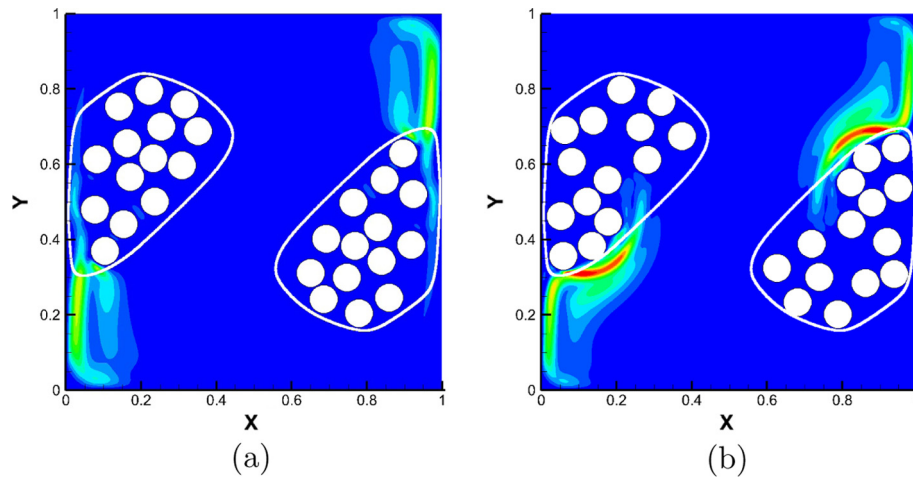


Fig. 7. Two configurations characterized by approximately the same porosity, $\phi \approx 0.59$, and different thermal insulating capacities: (a) $\overline{Nu} = 6.3393$; (b) $\overline{Nu} = 3.9832$. All the results are obtained for $Ra = 2.15 \times 10^6$ for differentially heated square cavity. The colors correspond to the distribution of the control parameter **A**.

Table 2

Basic statistics for \overline{Nu} values obtained as a function of the cylinder diameter for each set of the 2D simulations. All of the results were obtained for approximately the same porosity $\phi \approx 0.59$ and $Ra = 2.15 \times 10^6$.

D_{cyl}	N_{cyl}	\overline{Nu}_{max}	\overline{Nu}_{min}	\overline{Nu}	σ
0.04	94	3.8086	3.4078	3.5491	0.012
0.06	42	4.4449	3.7187	4.0300	0.105
0.074	28	6.3393	3.9832	4.6759	0.755
0.1	16	7.0326	4.1557	4.9890	0.851
0.16	6	8.0419	3.6894	5.3500	2.004

configurations from the same set characterized by the intermediate porosity values, as summarized in Table 1. Fig. 5 quantifies the dependance of the average \overline{Nu} and the steady-unsteady critical Rayleigh, Ra_{cr} and oscillating frequency, ω_{cr} values on the number of embedded cylinders observed for the porous media patterns characterized by the maximal and minimal porosity values. Note that the similar monotonic decrease in \overline{Nu} and intermittent increase in Ra_{cr} values as a function of the number of embedded cylinders was observed in [31] for the porous media patterns modelled by unconnected packed beds of equi-sized cylinders. It is interesting that although \overline{Nu} monotonically decreases, non-monotonic behavior is observed for Ra_{cr} and ω_{cr} , which could be related to the non-linearity of the system and reflects different physical branches existing for the same parameters. Note also that both critical values $Ra_{cr} = 2.15 \times 10^6$ and $\omega_{cr} = 1.606$ values obtained for the configuration without embedded cylinders ($N = 0$) are in a good agreement with the corresponding values reported in literature (see e.g. [44]).⁵ In the next step, the coordinates of the geometric centers of each of the 10 patterns were calculated by taking a weighted average of the positions and the areas of all the voids constituting the corresponding pattern. A further averaging of all the contours confining the obtained patterns and of the coordinates of the corresponding geometric centers yielded the averaged shape and position of the two final porous medium implants, as shown in Fig. 6. In the following we present the insulating capacity of the constructed implant of porous medium characterized by the average porosity value, as well as its validation for the realistic 3D flows.

3.2. Insulating properties and 3D validation of patterns modelled by unconnected packed beds of equi-sized cylinders

We start by constructing the next set of patterns filled with equi-sized cylinders of diameter $D = 0.074$, which is equal to the weighted average of the diameters of all the cylinders involved in the previous set of porous medium implants. All the patterns from this set are confined by the contour shown in Fig. 6 and are characterized by porosities approximately equal to $\phi \approx 0.5925$, which is the average porosity of all the patterns from the previous set.⁶ For all the patterns the maximal deviation between the target and the actual porosity values did not exceed 5%. The set comprises a special case of a more general configuration, analyzed in the previous section, and aims to address the question of whether the porosity of the modelled porous implant is the dominant parameter determining its insulating capacity. The insulating efficiency of the obtained patterns was next analyzed by calculating the average \overline{Nu} value for the vertical boundaries of the differentially heated cavity at $Ra = 2.15 \times 10^6$. This value corresponds to the value of the critical Ra number for the square differentially heated cavity without obstacles. The obtained results did not reveal a clear trend, indicating that porosity is the only parameter determining the insulating efficiency of the modelled porous implant. In contrast, the maximal and minimal values of the \overline{Nu} number ($\overline{Nu} = 6.3393$ and $\overline{Nu} = 3.9832$, respectively), comprising 77.2% and 48.5% of the \overline{Nu} value obtained for the configuration with no porous implants, were both obtained for the same porosity values (see Fig. 7). The high value of the standard

⁵ The present ω_{cr} value should be multiplied by \sqrt{Pr} to fit the time scaling of [44].

⁶ Note that in the most general case, a precise value of porosity cannot be exactly met by filling up the averaged contour with a discrete number of cylinders.

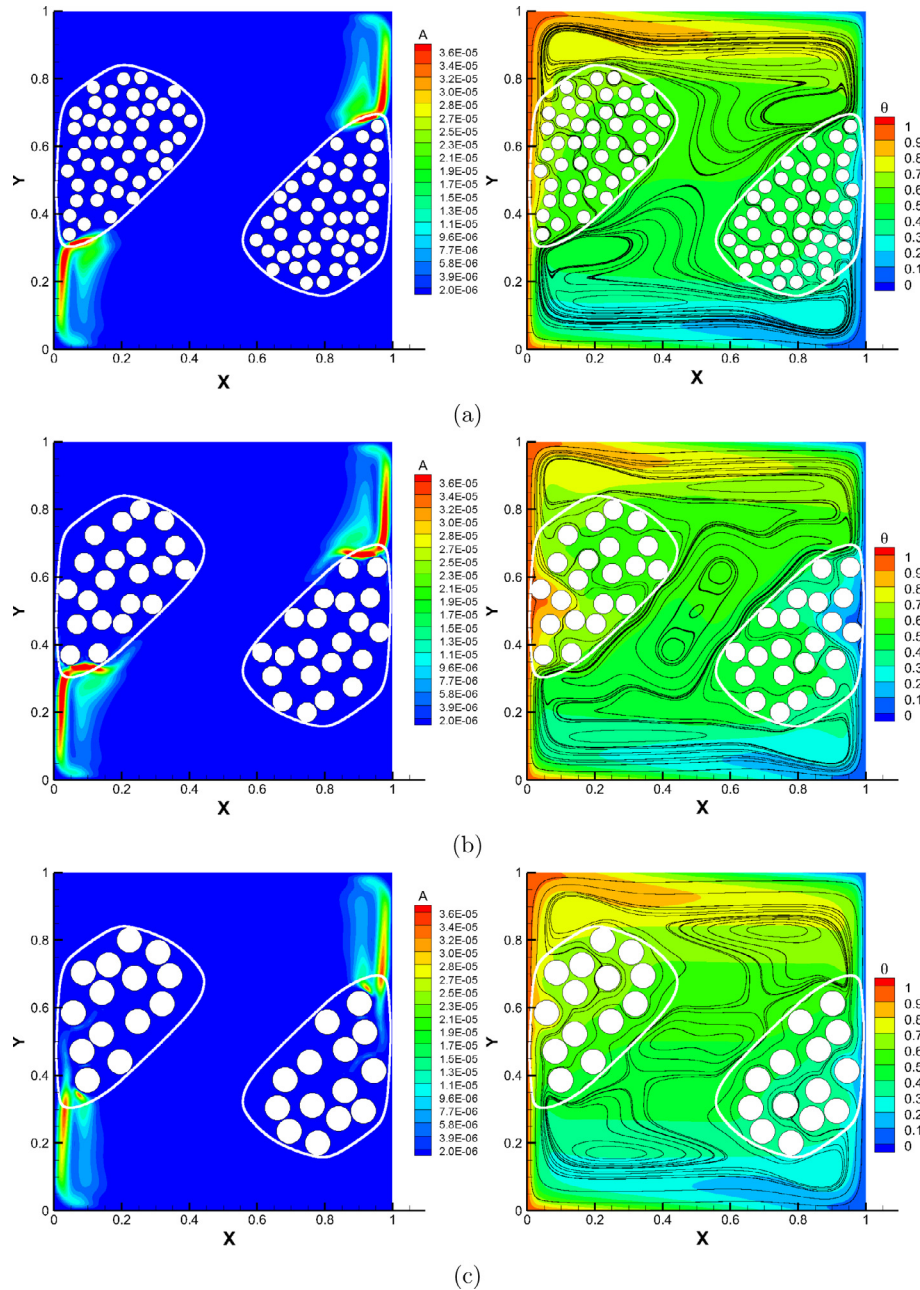


Fig. 8. Distribution of optimization parameter A (left graphs) and the corresponding temperature field (right graphs) with superimposed streamlines obtained for the implants characterized by approximately the same porosity, $\phi \approx 0.59$, for 2D flow. The implants embedded inside a square differentially heated cavity contain in total: (a) 94 cylinders; (b) 42 cylinders; (c) 28 cylinders; (d) 16 cylinders; (e) 6 cylinders.

deviation, $\sigma = 0.755$, obtained for the set of 10 different patterns also indicates a considerable scattering in the \bar{Nu} values.

To further investigate the impact of the cylinder diameter on the thermally insulating capacity of the modelled porous medium implant we constructed and simulated 4 more sets (10 patterns per each set) of porous media, each built of equi-sized unconnected cylinders. The diameter values of the cylinders, one for each set, were $D = 0.04, 0.06, 0.1, 0.16$, respectively. All the acquired results were used to obtain the basic statistics for \bar{Nu} values, as summarized in Table 2.

The porous medium implants built of cylinders of smaller diameters exhibit higher insulating capacity, as a result of the decrease

in the average values of \bar{Nu} with the cylinder diameter. However, more importantly for increasing the insulating capacity is the rapid decrease in the standard deviation value, σ , that indicates that the porous medium implants filled with randomly positioned cylinders of smaller diameters are more successful in reproducing the same thermally insulating capacity when compared to the implants consisting of larger cylinders. A physical explanation of the observed phenomenon can be found by looking at the contours of the optimization parameter A and the corresponding temperature distributions superimposed by streamlines, obtained for representative porous media patterns (see Fig. 8). The patterns shown in Fig. 8 have the \bar{Nu} number which is closest to the averaged \bar{Nu} value from the same set.

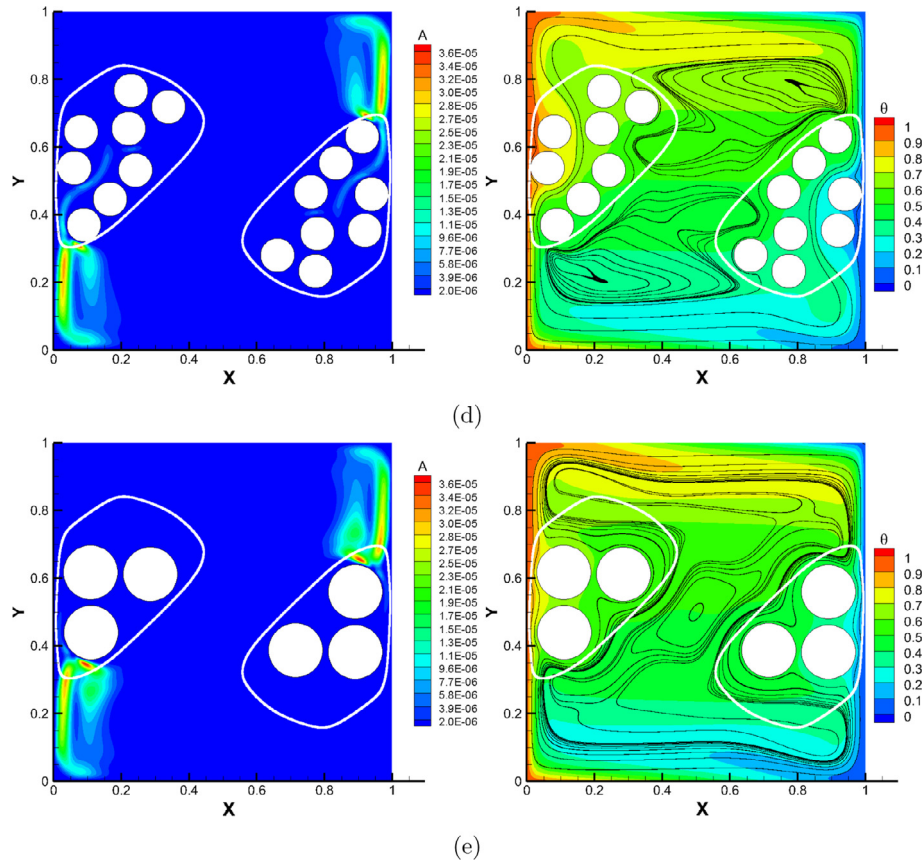


Fig. 8 (continued)

There are no significant differences between the distributions of parameter A for various patterns (see Fig. 8). This is in contrast to the distributions of the flow temperature and streamlines. It can be seen that the implants built of smaller cylinders are uniformly permeable to the convective flow. As the flow infiltrates through the implants it slows down and redistributes evenly. As a result, the temperature distribution inside the implants is almost uniform, which provides their high insulation capacity. On the other hand, the implants built of the larger cylinders are characterized by a non-uniform permeability. In the vicinity of cylindrical obstacles the implants are almost impermeable and only redirect the flow. However, the flow succeeds in penetrating the implants in the outermost regions. Despite decreasing when changing direction, the flow velocity still high and non-uniform inside a considerable part of the implants. As a result, high values of the temperature gradients are found in these regions, which significantly deteriorates the insulating efficiency of the implants.

To validate the observed trends we performed numerical simulations of realistic 3D flows by extending all the 2D configurations discussed above in the direction normal to the plane of the 2D cavity. As a result, the original 2D configurations are transformed into their 3D analogs (see Fig. 9), comprising cubic differentially heated cavities with perfect thermally conducting lateral walls and no-slip boundaries. The 2D circular obstacles are, in turn, transformed into 3D circular cylinders, extending in a spanwise direction over the entire width of the cavity.

Based on the simulation results, the \overline{Nu} values of all the configurations were then obtained for both 400^3 and 500^3 grid resolutions. Since our method is of second order accuracy, the zero grid size limit for the \overline{Nu} value was estimated by applying the Richard-

son extrapolation for two consequent grids. All the results are summarized in Table 3.

It is remarkable that the 3D results demonstrate the same trend that was observed for the 2D simulations: the implants built of smaller cylinders provide better thermal insulation and yield lower \overline{Nu} values. The \overline{Nu} values continuously rise with an increase in the cylinder diameters. The difference between the maximal and minimal \overline{Nu} values (for approximately the same porosities) for 3D flow is about 22%. This is somewhat lower than the corresponding value obtained for the 2D flow, which is about 50%. The difference stems from the much lower \overline{Nu} value predicted by the 2D simulations for implants built of the cylinders of the smallest diameter, which may be a result of the 2D idealization of the convective flow.

Recalling that the paper addresses the application of the developed method to the thermal insulation of construction blocks, we investigate the sensitivity of the patterns obtained to the opposite temperature difference. In other words, we address the question of whether the thermally insulated construction block will be as efficient in both hot and cold seasons (for both air conditioned and heated indoors) with the enhanced thermal insulation obtained by the proposed method. Table 4 shows the results summarizing the differences in \overline{Nu} values obtained for one of the representative configurations of the porous medium implants from each set of 2D configurations and the corresponding 3D analog. No significant differences can be seen for all the cases checked. The deviations do not exceed 10% and 4% for 2D and 3D configurations, respectively. It is remarkable that for both 2D and 3D flows the maximal differences in \overline{Nu} values are observed for implants built of smaller cylinders, which are characterized by the maximal insulation efficiency.

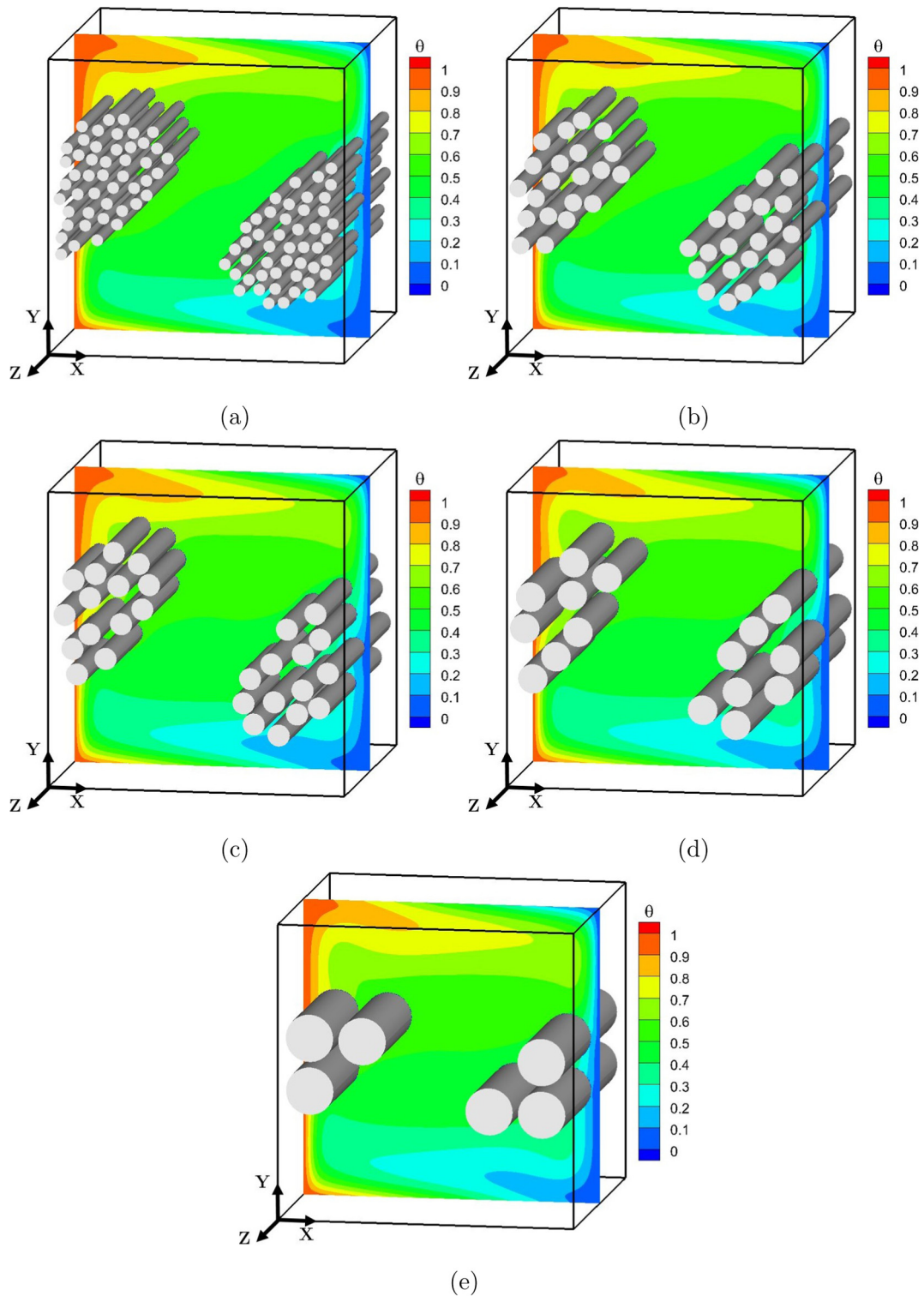


Fig. 9. Distribution of temperature field in the mid-cross-section of a 3D cavity obtained for the implants characterized by approximately the same porosity, $\phi \approx 0.59$, for 3D flow. The implants contain in total: (a) 94 cylinders; (b) 42 cylinders; (c) 28 cylinders; (d) 16 cylinders; (e) 6 cylinders.

Table 3
 \bar{Nu} values obtained for 400^3 , 500^3 grids and the \bar{Nu} value corresponding to the zero grid size limit estimated by the Richardson extrapolation.

D_{cyl}	N_{cyl}	\bar{Nu} (grid 400^3)	\bar{Nu} (grid 500^3)	\bar{Nu} (Richardson extrap.)
0.04	94	4.7727	4.9899	5.3761
0.06	42	5.2666	5.5046	5.9277
0.074	28	5.9388	6.1333	6.4792
0.10	16	5.6794	5.8894	6.2627
0.16	6	6.0119	6.2189	6.5868

Table 4

Nu deviation values, for the implants pre described in Table 3, between the presented physical model and the case of vertical wall temperature replacement (implants throughout this study are based on the clockwise flow circulation, temperature replacement causes the flow to pass through the existing implant in a counter clockwise circulation inside the cavity) for 2D and 3D.

D_{cyl}	N_{cyl}	Deviation in \overline{Nu} value (2D flow) [%]	Deviation in \overline{Nu} value (3D flow) [%]
0.04	94	9.37	3.34
0.06	42	4.72	3.79
0.074	28	4.78	0.34
0.1	16	3.88	0.40
0.16	6	3.31	0.16

4. Summary and conclusions

The concept of “smart” thermally insulating materials based on thermally passive porous media was generalized and extensively validated in the context of decreasing convective heat flux through the air filled cavities of hollow construction blocks. The porous medium was modelled by unconnected packed beds of circular cylinders. The basic statistical analysis treated the impact of a set of porous medium structures, consisting of both equi-sized and non-equi-sized cylinders, on the insulating efficiency of the porous media implants. The generalized geometry of the optimized porous medium implant and its spatial position inside a square differentially heated cavity (modelling the cavity located in the mid-core of construction block) were determined. It was demonstrated that optimally shaped porous media implants installed in accordance with the developed optimization methodology would occupy no more than 30% of the overall volume of the hollow brick cavity.

Regarding the major research questions related to the material properties of the modelled porous media which have been addressed in the present study it may be concluded that:

- The porosity is not the dominant parameter determining the insulating efficiency of the porous implant. Although the explicit determination of the permeability tensor of the porous medium implants remained out of the scope of the present study, it was shown that the thermal insulating efficiency of the implants is strongly correlated with their ability to slow down and to uniformly redistribute the infiltrating flow. A more explicit analysis of the permeability of the modelled porous media will be the focus of our future work.
- The precise positioning of the cylinders in accordance with the optimization parameter **A** inside the porous medium of the given porosity is not mandatory. The implants modelled by the randomly positioned small size cylinders exhibit consistent insulating efficiency. On the other hand, it was observed that the variance in the insulating efficiency of the implants increases with the diameter of the cylinders which form the porous medium implant modelled by unconnected packed beds.
- The porous medium implants modelled by unconnected packed beds of cylinders of smaller diameters are characterized by homogeneous internal patterns and succeed in consistently reproducing the same insulating efficiency. For this reason, among all the available porous materials only those characterized by a homogeneous internal pattern should be used when producing the optimized porous medium implants.

The results obtained by 2D analysis were extensively validated for realistic 3D flows. The 3D results exhibited the same trends as their 2D analogs, indicating an improvement in the insulating efficiency of the implants built of the cylinders of the smaller diameter. An acceptable 64% decrease in the \overline{Nu} value was predicted by

the 3D analysis of the flow inside the cubic differentially heated cavity with imbedded porous implants, compared to the original non-insulated configuration. It was also verified that the developed “smart” porous medium insulation is not sensitive to the opposite temperature difference; thus the insulating efficiency of construction blocks will remain the same in both hot and cold weather conditions.

Appendix A. Building confinement contours

All the confinement contours built in the framework of the present study comprise closed Bezier curves of the third order. The Bezier curve is a method widely used in computational graphics to create smooth curves by a series of control points. The number of control points determining the order of Bezier curve is arbitrary and is typically determined by the constraints posed by a specific engineering configuration. Typical examples of Bezier curves of the second and third order are shown in Fig. A.1a and b, respectively. The series of control points determining the curves are P_0 through P_2 for the second and P_0 through P_3 for the third order curves, respectively. Note that only the edge points from the given series belong to the Bezier curve itself,⁷ while all intermediate points only effect its slope and curvature. In practice, a Bezier curve can be parameterized by introducing parameter t and applying the binomial theorem in the form of:

$$P(t) = \sum_{i=0}^n \binom{n}{i} (1-t)^{n-i} t^i P_i, \quad (\text{A.1})$$

where

$$\binom{n}{i} = \frac{n!}{i!(n-i)!}, \quad (\text{A.2})$$

where n determines the order of the Bezier curve and P_i corresponds to the (X, Y) coordinates of the i th control point. All the Bezier curves built in the framework of the present study were based on the linear variation of parameter t (in general t does not have to vary linearly) in the interval of $t \in [0, 1]$. The final shape of the Bezier curve confining the implant of the porous medium was obtained by an iterative procedure based on the Anti-Grain Geometry open source library.⁸

Appendix B. Estimation of dimensions of realistic hollow construction blocks

Recalling that the current study was performed based on a non-dimensional analysis, it would be of practical interest to relate to the dimensions of realistic construction blocks, to which the developed method of “smart” thermal insulation could be applied. Without loss of generality we will assume that the cavity located in the mid-core of the construction block is of cubic geometry. We will next estimate the range of the cavity edge length, L , for the given range of temperature difference, $20 \text{ K} \leq \Delta T \leq 40 \text{ K}$, between the indoor and the outdoor environment. Note that the final dimensions of the construction block, including the wall and the bottom thicknesses, should take into account features inherent to the manufacturing process and comply with the requirements imposed on the strength of the block.

The expression for the length L can be obtained from the definition of the Ra number as $L = \sqrt[3]{\frac{Ra \cdot \nu^2}{g \beta \Delta T}}$. Taking the physical properties of dry air at $T = 300 \text{ K}$ we get the values of

⁷ A Bezier curve is intrinsically tangential to both lines passing through the edge points.

⁸ <http://www.antigrain.com/>.

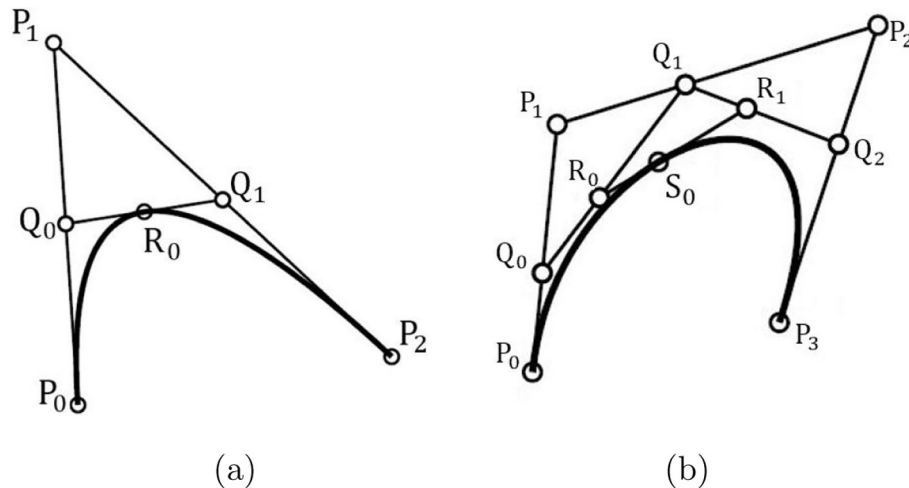


Fig. A.1. Typical Bezier curves of the second and third order. Intermediate points R_i , S_i and Q_i are obtained for the value of $t = 0.5$ [45].

$v = 1.568 \times 10^{-5} \left[\frac{\text{m}^2}{\text{sec}} \right]$, $\alpha = 22.07 \times 10^{-6} \left[\frac{\text{m}^2}{\text{sec}^2} \right]$, $\beta = \frac{1}{\tau} = \frac{1}{300} \left[\frac{1}{\text{K}} \right]$. We next recall that the non-dimensional analysis was performed for the value of $Ra = \frac{g\beta}{\nu\alpha} \Delta T L^3 = 2.15 \times 10^6$ and that the value of gravitational acceleration g is equal to $g = 9.81 \frac{\text{m}}{\text{sec}^2}$. Substitution of all the above values into the expression for L yields the characteristic dimensions of $L \approx 0.1$ [m] and for $\Delta T = 20$ K and $L \approx 0.08$ [m] for $\Delta T = 40$ K, which are typical of realistic construction blocks.

References

- [1] C. Balars, K. Droutsa, A. Argiriou, D. Asimakopoulos, Potential for energy conservation in apartment buildings, *Energy Build.* 31 (2000) 143–154.
- [2] Y. Feng, Thermal design standards for energy efficiency of residential buildings in hot summer/cold winter zones, *Energy Build.* 36 (2004) 1309–1312.
- [3] M. Ciampi, F. Leccese, G. Touni, Ventilated facades energy performance in summer cooling of buildings, *Sol. Energy* 75 (2003) 491–502.
- [4] L.M. Al-Hadhrami, A. Ahmad, Assessment of thermal performance of different types of masonry bricks used in Saudi Arabia, *Appl. Therm. Eng.* 29 (2009) 1123–1130.
- [5] V.A.F. Costa, Improving the thermal performance of red clay holed bricks, *Energy Build.* 70 (2014) 352–364.
- [6] T. Shimizu, K. Matsuura, H. Furue, K. Matsuzak, Thermal conductivity of high porosity alumina refractory bricks made by a slurry gelation and foaming method, *J. Eur. Ceram. Soc.* 33 (2013) 3429–3435.
- [7] M. Sutcu, A. Sedat, The use of recycled paper processing residues in making porous brick with reduced thermal conductivity, *Ceram. Int.* 35 (2009) 2625–2631.
- [8] M.A. Antar, Thermal radiation role in conjugate heat transfer across a multiple-cavity building block, *Energy* 35 (2010) 3508–3516.
- [9] M. Sutcu, J.J. del Coz Díaz, F.P. Á. Rabanal, O. Gencel, S. Akkurt, Thermal performance optimization of hollow clay bricks made up of paper waste, *Energy Build.* 75 (2014) 96–108.
- [10] T.W. Tong, F.M. Gerner, Natural convection in partitioned air-filled rectangular enclosures, *Int. Commun. Heat Mass Transf.* 13 (1986) 99–108.
- [11] A. Kangni, R. Ben Yedder, E. Bilgen, Natural convection and conduction in enclosures with multiple vertical partitions, *Int. J. Heat Mass Transf.* 34 (1991) 2819–2825.
- [12] A. Bouchair, Steady state theoretical model of fired clay hollow bricks for enhanced external wall thermal insulation, *Build. Environ.* 43 (2008) 1603–1618.
- [13] J.J. del Coz Díaz, N.P.J. García, S.J.L. Suárez, C. Betegón Biempica, Nonlinear thermal optimization of external light concrete multi-holed brick walls by the finite element method, *Int. J. Heat Mass Transf.* 51 (2008) 1530–1541.
- [14] J.J. del Coz Díaz, N.P.J. García, S.J.L. Suárez, S.I. Peñuelas, Non-linear thermal optimization and design improvement of a new internal light concrete multi-holed brick walls by FEM, *Appl. Therm. Eng.* 28 (2008) 1090–1100.
- [15] J.J. del Coz Díaz, P.J. García Nieto, J. Domnguez Hernández, A. Suárez Sánchez, Thermal design optimization of lightweight concrete blocks for internal one-way spanning slabs floors by FEM, *Energy Build.* 41 (2009) 1276–1287.
- [16] L.P. Li, Z.G. Wu, Z.Y. Li, Y.L. He, W.Q. Tao, Numerical thermal optimization of the configuration of multi-holed clay bricks used for constructing building walls by the finite volume method, *Int. J. Heat Mass Transf.* 51 (2008) 3669–3682.
- [17] M.A. Antar, H. Baig, Conjugate conduction–natural convection heat transfer in a hollow building block, *Appl. Therm. Eng.* 29 (2009) 3716–3720.
- [18] Y. Varol, H.F. Oztop, I. Pop, Natural convection in a diagonally divided square cavity filled with a porous medium, *Int. J. Therm. Sci.* 48 (2009) 1405–1415.
- [19] M.M. Alhazmy, Numerical investigation on using inclined partitions to reduce natural convection inside the cavities of hollow bricks, *Int. J. Therm. Sci.* 49 (2010) 2201–2210.
- [20] M.M. Alhazmy, Analysis of coupled natural convection–conduction effects on the heat transport through hollow building blocks, *Energy Build.* 38 (2006) 515–521.
- [21] D.L. Tang, L.P. Li, C.F. Song, W.Q. Tao, Y.L. He, Numerical thermal analysis of applying insulation material to holes in hollow brick walls by the finite-volume method, *Numer. Heat Transf. Part A* 68 (2015) 526–547.
- [22] E. Bilgen, Natural convection in enclosures with partial partitions, *Renew. Energy* 26 (2002) 257–270.
- [23] A.A. Merrikh, J.L. Lage, Natural convection in an enclosure with disconnected and conducting solid blocks, *Int. J. Heat Mass Transf.* 48 (2005) 1361–1372.
- [24] E.J. Braga, M.J.S. de Lemos, Laminar natural convection in cavities filled with circular and square rods, *Int. Commun. Heat Mass Transf.* 32 (2005) 1289–1297.
- [25] E.J. Braga, M.J.S. de Lemos, Heat transfer in enclosures having a fixed amount of solid material simulated with heterogeneous and homogeneous models, *Int. J. Heat Mass Transf.* 48 (2005) 4748–4765.
- [26] O. Laguerre, S. Benamara, D. Remy, D. Flick, Experimental and numerical study of heat and moisture transfers by natural convection in a cavity filled with solid obstacles, *Int. J. Heat Mass Transf.* 52 (2009) 5691–5700.
- [27] S.D. Jamalud-Din, D.A.S. Rees, B.V.K. Reddy, A. Narasimhan, Prediction of natural convection flow using network model and numerical simulations inside enclosure with distributed solid blocks, *Heat Mass Transf.* 46 (2010) 333–343.
- [28] S.L.M. Junqueira, F.C. De Lai, A.T. Franco, J.L. Lage, Numerical investigation of natural convection in heterogeneous rectangular enclosures, *Heat Transf. Eng.* 34 (2013) 460–469.
- [29] D. Iyi, R. Hasan, Natural convection flow and heat transfer in an enclosure containing staggered arrangement of blockages, *Procedia Eng.* 105 (2015) 176–183.
- [30] Y. Feldman, Y. Gulbeg, An extension of the immersed boundary method based on the distributed Lagrange multiplier approach, *J. Comput. Phys.* 322 (2016) 248–266.
- [31] Y. Gulbeg, Y. Feldman, Flow control through use of heterogeneous porous media: smart passive thermo-insulating materials, *Int. J. Therm. Sci.* 110 (2016) 369–382.
- [32] A.R. Martin, C. Saltiel, W. Shyy, Frictional losses and convective heat transfer in sparse, periodic cylinder arrays in cross flow, *Int. J. Heat Mass Transf.* 41 (1998) 2382–2397.
- [33] M.J. Keyser, M. Conradie, M. Coertzen, J.C. Van Dyk, Effect of coal particle size distribution on packed bed pressure drop and gas flow distributions, *Fuel* 85 (2006) 1439–1445.
- [34] A.S. Sangani, C. Yao, Transport process in random arrays of cylinders. II. Viscous flow, *Phys. Fluids* 31 (1988) 2435–2444.
- [35] A. Narvaez, K. Yazdchi, S. Luding, J. Harting, From creeping to inertial flow in porous media: a lattice boltzmann finite element study, *J. Stat. Mech. Theory Exp.* (2013) P02038.
- [36] D. Rochette, S. Clain, Two-dimensional computation of gas flow in porous bed characterized by a porosity jump, *J. Comput. Phys.* 219 (2006) 104–119.
- [37] C.S. Peskin, Flow patterns around heart valves: a numerical method, *J. Comput. Phys.* 10 (1972) 252–271.

- [38] M. Christon, P. Gresho, S. Sutton, Computational predictability of time-dependent natural convection flows in enclosures (including a benchmark solution), *Int. J. Numer. Meth. Fluids* 40 (2002) 953–980.
- [39] S. Xin, P. Le Quere, An extended Chebyshev pseudo-spectral benchmark for the 8:1 differentially heated cavity, *Int. J. Numer. Meth. Fluids* 40 (2002) 981–998.
- [40] A. Roma, C.S. Peskin, M.J. Berger, An adaptive version of the immersed boundary method, *J. Comput. Phys.* 153 (1999) 509–534.
- [41] A.Y. Gelfgat, Stability of convective flows in cavities: solution of benchmark problems by a low-order finite volume method, *Int. J. Numer. Meth. Fluids* 53 (2007) 485–506.
- [42] A. Gelfgat, Oscillatory Instability of Three-dimensional Natural Convection of Air in a Laterally Heated Cubic Box, 2015. Available from: <1508.00652>.
- [43] Y. Gulbeg, Y. Feldman, On laminar natural convection inside multi-layered spherical shells, *Int. J. Heat Mass Transf.* 91 (2015) 908–921.
- [44] S. Xin, L. Quere, Linear stability analyses of natural convection flows in a differentially heated square cavity with conducting horizontal walls, *Phys. Fluids* 13 (2001) 2529.
- [45] T.W. Sederberg, *Computer Aided Geometric Design Course Notes*, 2014.